applied sciences

MDPI

Article

Analytical Thermal Analysis of Radially Functionally Graded Circular Plates with Coating or Undercoating under Transverse and Radial Temperature Distributions

Yen-Ling Chung * and Zong-Han Lin †

Department of Construction Engineering, National Taiwan University of Science and Technology, Section 4, 43 Keelung Road, Taipei 106335, Taiwan
* Correspondence: chungyl@mail.ntust.edu.tw; Tel.: +886-2-2737-6558; Fax: +886-2-2737-6606
† Graduate student.

Abstract: This study aims to provide analytical solutions for circular plates coated or undercoated with functionally graded materials (FGMs) having Young's modulus functionality through the radius. The circular plates are subjected to thermal loads in radial and thickness directions. Because of the uncoupled stretching–bending problem of the radially FGM circular plate, the bending equilibrium equations in terms of displacements of the FGM-coated or -undercoated circular plates with Young's modulus based on the power–law function were established individually. General solutions for the homogeneous portion or FGM ring of the radially FGM-coated or -undercoated circular plate were developed separately. Subsequently, analytical thermal solutions for the radially FGM-coated or -undercoated circular plate were evaluated by solving the simultaneous boundary and continuity conditions equations. The analytical results were validated by comparing them with finite element solutions. When degenerated, they coincided with those of the homogeneous circular plate in the literature, enhancing the obtained solutions' reliability. These analytical solutions provide valuable insights into the plates' responses and expand the understanding of their mechanical behaviors under thermal loads. Furthermore, the effects of the FGM thickness, the material index, and the thermal loading conditions on the mechanical behaviors were under investigation. This parameter study offers valuable perspectives into the influence of these factors on the plate's structural response and aids in the optimization and design of FGM-coated or -undercoated circular plates.

Keywords: radially FGM-coated circular plate; radially FGM-undercoated circular plate; thermal-bending analytical solution; finite element solution

Citation: Chung, Y.-L.; Lin, Z.-H. Analytical Thermal Analysis of Radially Functionally Graded Circular Plates with Coating or Undercoating under Transverse and Radial Temperature Distributions. *Appl. Sci.* **2023**, *13*, 7061. https://doi.org/10.3390/app13127061

Academic Editor: Victor Franco Correia

Received: 12 May 2023
Revised: 3 June 2023
Accepted: 7 June 2023
Published: 12 June 2023

1. Introduction

Functionally graded materials (FGMs) offer several advantages owing to their unique composition, wherein the volume fractions of the constituents gradually vary in specific profiles. FGMs offer effective resistance against high temperatures and substantial reduction in thermal stresses [1]. The literature concerning FGM plates under thermal loads has witnessed a rapid increase in recent times. Chung and Chang [2] derived series solutions for FGM plates with a continuously varying coefficient of thermal expansion along the thickness direction. These solutions were derived for FGM plates experiencing linear temperature variations in the z-direction. Chung [3] extended the analysis to obtain closed-form solutions for FGM plates with temperature changes in both the x- and z-directions. The study demonstrated that by appropriately selecting material gradation from the derived closed-form solution, the deflection of the FGM plate in the thickness direction can be effectively minimized under thermal loading. In the study conducted by Golmakani [4], a comprehensive analysis was presented for shear deformable FGM plates under thermo-mechanical loads. The analysis considered different boundary conditions and employed a first-order shear deformation plate theory and the von Karman equations to accurately capture large deflections. Dai et al. [5] investigated the thermoelastic solution of a clamped-circular thin FGM plate by utilizing the classical plates theory. Their findings highlighted the significant impact of factors on the thermoelastic behavior of the FGM circular plate during transient conditions. Parandvar and Farid [6] explored the large amplitude vibration behavior of functionally graded plates under the influence of thermal load and random pressure. Alibeigloo [7] conducted a bending solution of a sandwich circular plate undercoated with a functionally graded layer under the combined thermal and mechanical loadings. The study employed the generalized differential quadrature method for the analysis. Ding and Wu [8] developed a hybrid optimization approach, combining a genetic algorithm with a complex method. The objective was to optimize the material constitution of a multi-layered FGM plate. Zhang et al. [9] examined the dynamic thermal buckling and post-buckling behavior of annular plates made of imperfect FGMs, using principles from the nonlinear plate theory. Zarga et al. [10] utilized a straightforward quasi-3D shear deformation theory to analyze the thermo-mechanical bending characteristics of sandwich plates composed of functionally graded materials. The researchers investigated the influence of the thermal load, geometric parameters, and gradient index on the bending response of the FGM sandwich plates. A detailed investigation was carried out by Vaghefi [11] to analyze the thermo-elastoplastic bending response of sandwich plates characterized by functionally graded (FG) face sheets and a combination of FG and homogeneous core materials. The research conducted by Moleiro et al. [12] focused on the multi-objective design optimization of FGM plates, consisting of a primary layer made of FGM, with the possibility of including metal and/or ceramic faces. Considering the temperature dependence of material properties is crucial in the thermal analysis of FGMs, particularly in the context of thermal buckling [13–15]. Furthermore, researchers such as Akgöz and Civalek [16] have examined the thermal vibration behavior of temperature-dependent FGM microbeams, while Javani et al. [17] have investigated annular FGM plates.

Among numerous studies on FGMs, an interesting issue is the FGM used as the coated or undercoated layers; this is attributed to the fact that incorporating FGMs as coated or undercoated layers in a sandwich or multi-layer plates results in remarkably uniform stress distributions between adjacent layers [18]. Stress intensity factors of composite media with cracked coating–substrate interfaces were investigated by Chi and Chung [19] utilizing the finite element method. The study highlighted the potential of FGM in mitigating stress singularities along the interfaces. Based on the Fourier series expansion method, Han et al. [20] conducted a comprehensive investigation on the buckling behavior of a cylindrical shell coated with FGM under thermal loading conditions. Mao et al. [21] simulated the sliding interaction between an FGM-coated half-plane and a homogeneous half-plane to investigate the frictional heat and thermal contact resistance in brake systems. The research findings showed that an appropriate choice of gradient type can effectively regulate the coupled thermoelastic instability observed in the sliding system. Utilizing the higher-order shear deformation plate theory, Daikh and Megueni [22] conducted a research study to explore the effects of various factors, such as the plate aspect ratio and thermal loading conditions, on the critical buckling temperature of FGM sandwich plates. Dung and Nga [23] presented a comprehensive analysis of the post-buckling characteristics of eccentrically stiffened sandwich plates supported on elastic foundations under different loading conditions based on Reddy's third-order shear deformation plate theory incorporating von Karman geometrical nonlinearity. Daikh et al. [24] employed a higher-order shear deformation theory and applied Hamilton's variational principle to investigate the free vibration characteristics of rectangular nanoplates with temperature-dependent FGM layers. Nguyen et al. [25] investigated the nonlinear static behaviors of sandwich plates on an elastic foundation, taking into account the temperature dependency of the FGM material. The investigation of the dynamic behavior of multi-directional porous sandwich plates consisting of two functionally graded face sheets and a homogeneous core was studied by Kumar and Ghosh [26] using Navier's solution technique.

FGMs are microscopically inhomogeneous with the material properties varying continuously from one surface to the other obeying certain functions. Over the past few decades, a considerable number of studies [27–30] corresponding to the FGM circular plates assumed the through-the-thickness FGM using either a power–law or exponential function. However, due to the phenomenon of the uncoupled stretching–bending problem of the through-the-radius FGM plate, the study of the radial FGM plate has been growing. Nie and Zhong [31] assumed the material properties varying in the radial direction to study the axisymmetric bending of functionally graded circular and annular plates. By considering a radial variation of Young's modulus employing a power–law relationship, Sburlati [32] proposed an analytical solution to address the issue of the stress concentration factor of an isotropic homogeneous plate with a circular hole, and Goyat et al. [33] suggested that selecting an appropriate material gradation model and power-law index can significantly mitigate stress concentration factors.

Although the radially FGM circular plates result in the uncoupled stretching–bending behavior, the bending equilibrium equation of the through-the-radius FGM circular plate is more complicated than that of the through-the-thickness FGM plate, and hence, only a limited number of analytical solutions have been derived for radially graded circular plates. To the best of the authors' knowledge, no thermal-bending analytical solution of the radially FGM-coated or FGM-undercoated circular plates has been reported. The point is that analytical solutions play a crucial role as reference benchmarks for researchers to validate the accuracy and reliability of their numerical methods. Therefore, the purpose of this study is to establish the analytical solutions for deflection, stresses, and moments of the radially FGM-coated or -undercoated circular plates under transversely and radially thermal loading.

2. The Governing Equation and General Solution

Consider a circular FGM plate with a moderate thickness, characterized by its radius R and thickness h, and subjected to an axisymmetric thermal load $T(r,z)$. The coordinates (r,θ,z) define the plane and the thickness directions of the circular FGM plate. The assumption made in this study is that Poisson's ratio of the circular plate remains constant, while Young's modulus varies radially based on a power function.

2.1. Governing Equations

While the through-the-radius FGM circular plates exhibit heterogeneity, their stretching and bending behaviors are decoupled due to mid-surface symmetry. Considering small deformations about the plate's thickness, the strains in the (r,θ,z) directions of the FGM circular plate expressed as bending displacements w are $\{\varepsilon_r,\ \varepsilon_\theta,\ \gamma_{r\theta}\} = z\{\kappa_r, \kappa_\theta, \kappa_{r\theta}\}$, where $\kappa_r,\ \kappa_\theta,\ \kappa_{r\theta}$ are curvatures of the FGM plate. For the non-homogeneous elastic FGM plate with Young's modulus $E(r)$ and Poisson's ratio ν, the stress–strain relation under thermal loading $T(r,z)$ based on the assumptions of small deformation can be described as follows [2]:

$$\begin{Bmatrix} \sigma_r \\ \sigma_\theta \\ \tau_{r\theta} \end{Bmatrix} = \frac{E(r)}{1-\nu^2}\begin{bmatrix} 1 & \nu & 0 \\ \nu & 1 & 0 \\ 0 & 0 & (1-\nu)/2 \end{bmatrix}\begin{Bmatrix} \varepsilon_r \\ \varepsilon_\theta \\ \gamma_{r\theta} \end{Bmatrix} - \frac{E(r)\alpha T(r,z)}{1-\nu}\begin{Bmatrix} 1 \\ 1 \\ 0 \end{Bmatrix} \tag{1}$$

where α is the thermal expansion coefficient. The definitions of the bending moments $(M_r, M_\theta, M_{r\theta}) = \int_{-h/2}^{h/2} (z\sigma_r, z\sigma_\theta, z\tau_{r\theta})dz$ yield

$$\begin{Bmatrix} M_r \\ M_\theta \\ M_{r\theta} \end{Bmatrix} = \frac{E(r)h^3}{12(1-\nu^2)}\begin{bmatrix} 1 & \nu & 0 \\ \nu & 1 & 0 \\ 0 & 0 & (1-\nu)/2 \end{bmatrix}\begin{Bmatrix} \kappa_r \\ \kappa_\theta \\ \kappa_{r\theta} \end{Bmatrix} - \begin{Bmatrix} M^{\Delta T} \\ M^{\Delta T} \\ 0 \end{Bmatrix}, \tag{2}$$

where the entry $M^{\Delta T}$ is of the following form:

$$M^{\Delta T} = \frac{\alpha E(r)}{1-\nu}\int_{-h/2}^{h/2} zT(r,z)dz. \quad (3)$$

The equilibrium equations in the r-, θ-, and z-directions of the elastic solid subjected to the transverse load q_z are [34]

$$\frac{\partial N_r}{\partial r} + \frac{\partial N_{r\theta}}{r\partial\theta} + \frac{N_r - N_\theta}{r} = 0,\ \frac{\partial N_{r\theta}}{\partial r} + \frac{\partial N_\theta}{r\partial\theta} + \frac{2}{r}N_{r\theta} = 0,\ \frac{\partial V_r}{\partial r} + \frac{V_r}{r} + \frac{1}{r}\frac{\partial V_\theta}{\partial\theta} = -q_z \quad (4)$$

where V_r and V_θ are the transverse shear forces acting on the radial and tangential surfaces, respectively, and they are

$$V_r = \frac{\partial M_r}{\partial r} + \frac{M_r - M_\theta}{r} + \frac{1}{r}\frac{\partial M_{r\theta}}{\partial\theta},\quad V_\theta = \frac{\partial M_{r\theta}}{\partial r} + 2\frac{M_{r\theta}}{r} + \frac{1}{r}\frac{\partial M_\theta}{\partial\theta}. \quad (5)$$

Substituting Equation (5) into Equation (4) gives the equilibrium equation in the z-direction in terms of the moments:

$$\frac{\partial^2 M_r}{\partial r^2} + \frac{2}{r}\frac{\partial^2 M_{r\theta}}{\partial r\partial\theta} + \frac{1}{r^2}\frac{\partial^2 M_\theta}{\partial\theta^2} + \frac{2}{r}\frac{\partial M_r}{\partial r} + \frac{2}{r^2}\frac{\partial M_{r\theta}}{\partial\theta} - \frac{1}{r}\frac{\partial M_\theta}{\partial r} = -q_z. \quad (6)$$

Further, assume that the FGM circular plate exhibits radial variations in its Young's modulus following the power function:

$$E(r) = E_0\left(\frac{r}{R}\right)^n. \quad (7)$$

In the absence of a transverse load q_z, the substitution of Equations (2)–(6), along with the assistance of Equation (3), results in the bending equilibrium equation for FGM circular plates with a through-the-radius variation of Young's modulus $E(r) = E_0(r/R)^n$, expressed in terms of displacement:

$$\begin{aligned}\frac{E_0h^3}{12(1-\nu^2)}\left(\frac{r}{R}\right)^n\Big\{\nabla^4 w + \frac{2n}{r}\frac{\partial^3 w}{\partial r^3} + \frac{n(n+1+\nu)}{r^2}\frac{\partial^2 w}{\partial r^2} + \frac{n(n\nu-\nu-1)}{r^3}\frac{\partial w}{\partial r} \\ + \frac{n(n\nu-\nu-3)}{r^4}\frac{\partial^2 w}{\partial\theta^2} + \frac{2n}{r^3}\frac{\partial^3 w}{\partial r\partial\theta^2}\Big\} = -\nabla^2 M^{\Delta T},\end{aligned} \quad (8)$$

where $\nabla^2 = \frac{\partial^2}{\partial r^2} + \frac{1}{r}\frac{\partial}{\partial r} + \frac{1}{r^2}\frac{\partial^2}{\partial\theta^2}$. Equation (8) reveals that the equilibrium equation for the radially FGM circular plate is more complex compared to that of the FGM circular plate with varying material properties in the thickness direction. In the case of axisymmetric bending, the deflections of the radially FGM circular plate remain independent of the angle θ, i.e., $w = w(r)$ and $\partial(\ )/\partial\theta = 0$. The bending equilibrium equation, Equation (8), can be simplified as:

$$\frac{h^3E_0}{12(1-\nu^2)}\left(\frac{r}{R}\right)^n\left\{\nabla^4 w + \frac{2n}{r}\frac{d^3w}{dr^3} + \frac{n(n+1+\nu)}{r^2}\frac{d^2w}{dr^2} + \frac{n(n\nu-\nu-1)}{r^3}\frac{dw}{dr}\right\} = -\frac{1}{r}\frac{dM^{\Delta T}}{dr} - \frac{d^2M^{\Delta T}}{dr^2}. \quad (9)$$

2.2. The General Solution

To assess the impact of temperature changes along the radial and thickness directions on the thermal mechanics of the radial FGM, two factors related to temperature distributions in these directions are taken into consideration. As a result, we assume a temperature distribution of the form $T(r,z) = T_0(1+\bar{r}^m)\bar{z}^{2P+1}$, where $\bar{r} = (r/R)$ and $\bar{z} = (z/h)$, and then the quantity $M^{\Delta T}$ in Equation (3) is

$$M^{\Delta T} = \frac{E_0h^3D}{12(1-v^2)}\bar{r}^n(1+\bar{r}^m),\ \text{where } D = \frac{12(1+v)\alpha T_0}{(2^{2P+2})(2P+3)h} \quad (10)$$

for the FGM circular plate with Young's modulus $E(r) = E_0\bar{r}^n$. It is evident that when $m = 0$ or $P = -0.5$, the temperature distributions are solely along the transverse or radial direction, respectively. Importantly, Equation (10) can be applied to a homogeneous plate by setting $n = 0$. To solve Equation (9), the setting $r = e^t$ enables us to reformulate it into an ordinary differential equation with constant coefficients, as shown below:

$$\begin{aligned}&\tfrac{d^4w}{dt^4} + (2n-4)\tfrac{d^3w}{dt^3} + \left[n^2 + (\nu-5)n + 4\right]\tfrac{d^2w}{dt^2} + n(\nu n - n - 2\nu + 2)\tfrac{dw}{dt} \\ &\quad = -D\left[n^2e^{2t} + (m+n)^2R^{-m}e^{(m+2)t}\right]\end{aligned}. \quad (11)$$

The homogeneous solution $w_h(t)$ of Equation (11) can be easily obtained by letting $w_h(t) = e^{\lambda t}$ and then substituting it into Equation (11), resulting in four roots which are

$$\lambda_1 = 0,\ \lambda_2 = 2-n,\ \lambda_3 = \frac{1}{2}\left(2-n-\sqrt{4+n^2-4n\nu}\right),\ \lambda_4 = \frac{1}{2}\left(2-n+\sqrt{4+n^2-4n\nu}\right).$$

It is obvious that λ_i have repeated roots for $n = 0$ and $n = 2$. Thereby, the homogeneous solution $w_h(r)$ is expressed as:

$$w_h(r) = \begin{cases} C_1 + C_2r^2 + C_3\ln r + C_4r^2\ln r & as\ n = 0 \\ C_1 + C_2r^{\lambda_2}\ln r + C_3r^{\lambda_3} + C_4r^{\lambda_4} & as\ n = 2 \\ C_1 + C_2r^{\lambda_2} + C_3r^{\lambda_3} + C_4r^{\lambda_4} & as\ n \neq 0\ or\ n \neq 2 \end{cases}. \quad (12)$$

Please note that Equation (12) is valid for $r \neq 0$, such as annular FGM plates. The first equation of Equation (12) can be applied to homogeneous circular plates. Whereas, the function $\ln r$ is not defined at $r = 0$, which corresponds to the center of the circular plate. To guarantee the existence of the bending solution of a circular plate, the coefficients C_3, C_4 must be zero and consequently, the homogeneous solution $w_h(r)$ for a homogeneous circular plate is

$$w_h(r) = C_1 + C_2r^2. \quad (13)$$

The particular solution to the Equation (11) is in the form of $w_p(t) = C_5e^{2t} + C_6e^{(m+2)t}$, and it is easy to obtain the coefficients C_5 and C_6 as

$$C_5 = 0,\ C_6 = \begin{cases} 0 & m = 0 \\ \frac{-D}{(2+m)^2R^m} & m \neq 0 \end{cases}. \quad (14)$$

for homogeneous circular plates, and

$$C_5 = \frac{-D}{2(1+\nu)},\ C_6 = \frac{-(m+n)^2D}{R^m\xi} \quad (15)$$

With $\xi = (m+2)^4 + (2n-4)(m+2)^3 + [n^2 + (\nu-5)n + 4](m+2)^2 + n(\nu n - n - 2\nu + 2)(m+2)$ for an FGM circular plate. Finally, the general solution of the radially FGM circular plate is then the sum of the homogeneous solution $w_h(r)$ and the particular solution $w_P(r)$.

3. Circular Plate Coated with Radially FGM

Here, a circular plate with radius R and height h coated with radially FGM subjected to thermal load $T(r,z) = T_0(1+\bar{r}^m)\bar{z}^{2P+1}$ is considered, as shown in Figure 1a. The inner region of the FGM-coated circular plate is characterized by homogeneity, with a constant Poisson's ratio ν and a uniform Young's modulus $E_0^* = E_0\overline{R}_1^n$ where $\overline{R}_1 = R_1/R$. On the other hand, the outer region of the FGM-coated circular plate consists of an FGM ring, with a constant Poisson's ratio ν and Young's modulus that varies radially based on a power function, i.e.,

$$E(r) = \begin{cases} E_0^* & 0 \le r \le R_1 \\ E_0(r/R)^n & R_1 \le r \le R \end{cases}. \tag{16}$$

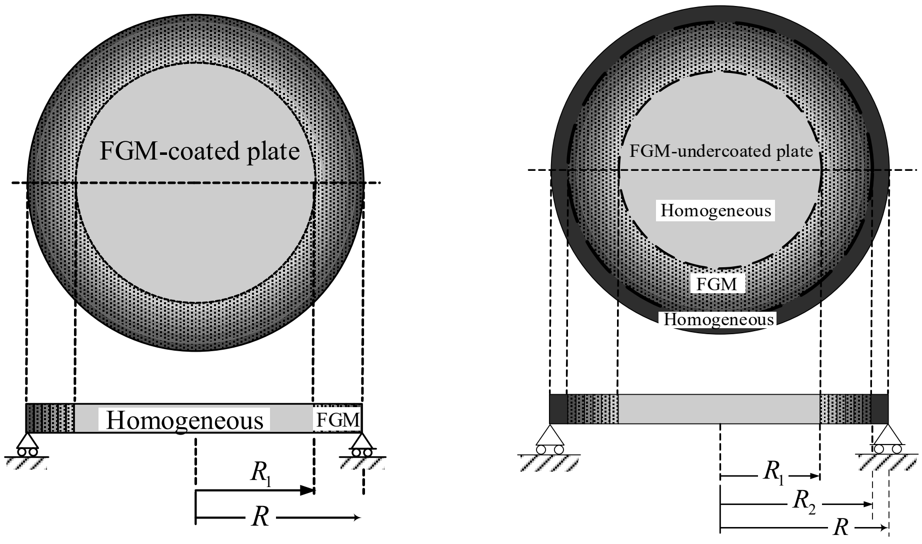

Figure 1. The configurations of the FGM-coated and the FGM-undercoated circular plates. (**a**) The FGM-coated circular plate; (**b**) the FGM-undercoated circular plates.

The general solution for each section of the FGM-coated circular plate can be obtained separately by directly applying the results from Section 2. It is important to highlight that while the Young's modulus $E_0^* = E_0\overline{R}_1^n$ within the range $0 \le r < R_1$ varies based on the material index n of the outer FGM-annular section, the inner portion of the FGM-coated circular plate represents a homogeneous circular plate with a uniform Young's modulus E_0^* for a specific value of n. Hence, Equation (13) can serve as the homogeneous solution for the inner portion of the FGM-coated circular plate.

3.1. The Homogeneous Portion of the FGM-Coated Circular Plate: $0 \le r < R_1$

Equations (13) and (14) are used as the general solution in the range $0 \le r < R_1$, i.e.,

$$w(r) = A_{11} + A_{12}r^2 + A_{16}r^{m+2} \tag{17}$$

where A_{11} and A_{12} are unknowns; the quantity A_{16} is the coefficient C_6, i.e., $A_{16} = 0$ for $m = 0$ and $A_{16} = -D/[(2+m)^2R^m]$ for $m \ne 0$. Consequently, the stresses and bending moments defined in Equations (1)–(3) are expressed as follows:

$$\begin{aligned} \sigma_r &= -\tfrac{zE_0^*}{1-\nu^2}[2(1+\nu)A_{12} + m_{\nu1}A_{16}r^m] - \tfrac{E_0^*\alpha T_0}{1-v}(1+\overline{r}^m)\overline{z}^{2P+1}, \\ \sigma_\theta &= -\tfrac{zE_0^*}{1-\nu^2}[2(1+\nu)A_{12} + m_{\nu2}A_{16}r^m] - \tfrac{E_0^*\alpha T_0}{1-v}(1+\overline{r}^m)\overline{z}^{2P+1}, \\ M_r &= -\tfrac{E_0^*h^3}{12(1-\nu^2)}[2(1+\nu)A_{12} + m_{\nu1}A_{16}r^m] - \tfrac{E_0^*h^3D}{12(1-v^2)}(1+\overline{r}^m), \\ M_\theta &= -\tfrac{E_0^*h^3}{12(1-\nu^2)}[2(1+\nu)A_{12} + m_{\nu2}A_{16}r^m] - \tfrac{E_0^*h^3D}{12(1-v^2)}(1+\overline{r}^m), \end{aligned} \tag{18}$$

where $m_{\nu1} = (m+2)(m+1+\nu)$, $m_{\nu2} = (m+2)(m\nu+1+\nu)$.

3.2. The FGM Annular Portion of the FGM-Coated Circular Plate: $R_1 \le r \le R$

The general solutions of the FGM annular portion can be directly established from Equations (12) and (14), and they are

$$w(r) = \begin{cases} A_{21} + A_{22}r^2 + A_{23}\ln r + A_{24}r^2 \ln r + A_{26}r^{m+2}, & \text{for } n = 0 \\ A_{21} + A_{22}r^{\lambda_2}\ln r + A_{23}r^{\lambda_3} + A_{24}r^{\lambda_4} + A_{25}r^2 + A_{26}r^{m+2}, & \text{for } n = 2 \\ A_{21} + A_{22}r^{\lambda_2} + A_{23}r^{\lambda_3} + A_{24}r^{\lambda_4} + A_{25}r^2 + A_{26}r^{m+2}, & \text{for } n \ne 0 \text{ or } n \ne 2 \end{cases} \quad (19)$$

where $A_{21},\ A_{22},\ A_{23},\ A_{24}$ are unknown constants; A_{25} and A_{26} are the coefficients of a particular solution, related to Equation (15) as

$$A_{25} = \frac{-D}{2(1+\nu)},\ A_{26} = \frac{-(m+n)^2 D}{R^m \xi}. \quad (20)$$

Consequently, the stresses and bending moments of the FGM annular portion evaluated according to Equations (1)–(3) are

$$\sigma_j = \sigma_{j1} - \sigma_{T1},\ M_j = \frac{h^3}{12z}\sigma_{j1} - M_{T1}, j = r, \theta \quad (21)$$

where

$$\begin{aligned} \sigma_{r1} &= -\tfrac{zE_0}{1-\nu^2}\left\{2(1+\nu)A_{22} + (\nu-1)A_{23}r^{-2} + [2(1+v)\ln r + \nu + 3]A_{24} + m_{\nu 1}A_{26}r^m\right\}, \\ \sigma_{\theta 1} &= -\tfrac{zE_0}{1-\nu^2}\left\{2(1+\nu)A_{22} + (1-v)A_{23}r^{-2} + [2(1+v)\ln r + 3v + 1]A_{24} + m_{\nu 2}A_{26}r^m\right\}, \\ \sigma_{T1} &= \tfrac{E_0\alpha T_0}{1-v}(1+\bar{r}^m)\bar{z}^{2P+1},\ M_{T1} = \tfrac{E_0 h^3 D}{12(1-v^2)}(1+\bar{r}^m) \end{aligned}$$

for $n = 0$,

$$\sigma_j = \sigma_{j2} - \sigma_{T2},\ M_j = \frac{h^3}{12z}\sigma_{j2} - M_{T2}, j = r, \theta \quad (22)$$

where

$$\begin{aligned} \sigma_{r2} &= -\tfrac{zE_0\bar{r}^2}{1-\nu^2}\left\{-(1-v)A_{22}r^{-2} + \lambda_{3\nu}A_{23}r^{\lambda_3-2} + \lambda_{4\nu}A_{24}r^{\lambda_4-2} + 2(1+v)A_{25} + m_{\nu 1}A_{26}r^m\right\}, \\ \sigma_{\theta 2} &= -\tfrac{zE_0\bar{r}^2}{1-\nu^2}\left\{(1-v)A_{22}r^{-2} + \lambda_{3\nu}A_{23}r^{\lambda_3-2} + \lambda_{4\nu}A_{24}r^{\lambda_4-2} + 2(1+v)A_{25} + m_{\nu 2}A_{26}r^m\right\}, \\ \sigma_{T2} &= \tfrac{E_0\bar{r}^2\alpha T_0}{1-v}(1+\bar{r}^m)\bar{z}^{2P+1},\ M_{T2} = \tfrac{E_0\bar{r}^2 h^3 D}{12(1-v^2)}(1+\bar{r}^m) \end{aligned}$$

with $\lambda_3 = -\sqrt{2-2\nu}$, $\lambda_4 = \sqrt{2-2\nu}$ for $n = 2$, and

$$\sigma_j = \sigma_{j3} - \sigma_{T3},\ M_j = \frac{h^3}{12z}\sigma_{j3} - M_{T3}, j = r, \theta \quad (23)$$

where

$$\begin{aligned} \sigma_{r3} &= -\tfrac{zE_0\bar{r}^n}{1-\nu^2}\left\{\lambda_{2\nu}A_{22}r^{\lambda_2-2} + \lambda_{3\nu}A_{23}r^{\lambda_3-2} + \lambda_{4\nu}A_{24}r^{\lambda_4-2} + 2(1+v)A_{25} + m_{\nu 1}A_{26}r^m\right\}, \\ \sigma_{\theta 3} &= -\tfrac{zE_0\bar{r}^n}{1-\nu^2}\left\{\lambda^*_{2\nu}A_{22}r^{\lambda_2-2} + \lambda^*_{3\nu}A_{23}r^{\lambda_3-2} + \lambda^*_{4\nu}A_{24}r^{\lambda_4-2} + 2(1+v)A_{25} + m_{\nu 2}A_{26}r^m\right\}, \\ \sigma_{T3} &= \tfrac{E_0\bar{r}^n\alpha T_0}{1-v}(1+\bar{r}^m)\bar{z}^{2P+1},\ M_{T3} = \tfrac{E_0\bar{r}^n h^3 D}{12(1-v^2)}(1+\bar{r}^m) \end{aligned}$$

with $\lambda_{2\nu} = \lambda_2(\lambda_2 - 1 + v)$, $\lambda_{3\nu} = \lambda_3(\lambda_3 - 1 + v)$, $\lambda_{4\nu} = (\lambda_4 - 1 + v)$, and $\lambda^*_{2\nu} = \lambda_2(\nu\lambda_2 - \nu + 1)$, $\lambda^*_{3\nu} = \lambda_3(\nu\lambda_3 - \nu + 1)$, $\lambda^*_{4\nu} = \lambda_4(\nu\lambda_4 - \nu + 1)$ for $n \ne 0$ or $n \ne 2$.

Importantly, a notable observation is that in the special case of $P = 0$, which signifies a linear temperature variation along the thickness direction, the relationships $M_{Tj} = h^3\sigma_{Tj}/(12z), j = 1,\ 2,\ 3$ in Equations (21)–(23) are valid. Consequently, the thermal stresses and moments exhibit the relationships $M_j = h^3\sigma_j/(12z)$, $j = r,\ \theta$ for this specific case of $P = 0$.

3.3. The Analytical Solution of the FGM-Coated Circular Plate

The six unknown constants including A_{11},A_{12} of the homogeneous circular portion, and A_{21}, A_{22}, A_{23}, A_{24} of the FGM-coated annular portion can be obtained by considering the boundary conditions and continuity equations:

$$\begin{aligned}&w(r=R)=0,\ M_r(r=R)=0,\ w(r=R_1^-)=w(r=R_1^+),\ \left.\frac{dw}{dr}\right|_{r=R_1^-}=\left.\frac{dw}{dr}\right|_{r=R_1^+},\\&M_r(r=R_1^-)=M_r(r=R_1^+),\ V_r(r=R_1^-)=V_r(r=R_1^+).\end{aligned}\tag{24}$$

Equation (24) provides six simultaneous equations to solve six unknowns as follows:

(1) For $n=0$

When $n=0$, the FGM-coated circular plate degenerates to the homogeneous circular plate with Young's modulus E_0. The six unknowns A_{11}, A_{12}, A_{21}, A_{22}, A_{23}, A_{24} for the case $n=0$ are evaluated from Equation (24). Substituting the obtained coefficients into Equation (17) or Equation (19), one can find the bending deflection of a homogeneous circular plate under thermal load $T(r,z)=T_0(1+\bar{r}^m)\bar{z}^{2P+1}$ as:

$$w(r)=\frac{DR^2}{2(1+\nu)}\left\{\frac{m+3-v}{m+2}\left(1-\bar{r}^2\right)+\frac{2(1+v)}{(m+2)^2}\left(1-\bar{r}^{m+2}\right)\right\}.\tag{25}$$

Notably, Equation (25) coincides with that presented by Hetnarski [34]. Subsequently, the stresses and bending moments of the homogeneous circular plate under thermal loads are

$$\begin{aligned}\sigma_r&=\tfrac{zE_0D}{(m+2)(1-v^2)}[(m+3-v)+(m+1+v)\bar{r}^m]-\tfrac{E_0\alpha T_0}{1-v}(1+\bar{r}^m)\bar{z}^{2P+1},\\\sigma_\theta&=\tfrac{zE_0D}{(m+2)(1-v^2)}\{(m+3-v)+(mv+v+1)\bar{r}^m\}-\tfrac{E_0\alpha T_0}{1-v}(1+\bar{r}^m)\bar{z}^{2P+1},\\M_r&=\tfrac{E_0h^3D}{12(m+2)(1+\nu)}(1-\bar{r}^m),\\M_\theta&=\tfrac{E_0h^3D}{12(m+2)(1+\nu)}[1-(m+1)\bar{r}^m].\end{aligned}\tag{26}$$

(2) For $n=2$

The coefficients A_{11}, A_{12}, A_{21}, A_{22}, A_{23}, A_{24} for $n=2$ determined from the simultaneous equations of boundary and continuity conditions are expressed in the form as follows:

$$\{A_{11},\ A_{12},\ A_{21},\ A_{22},\ A_{23},\ A_{24}\}^T=[K]^{-1}\{K_1\}$$

herein

$$[K]=\begin{bmatrix}0&0&-1&-\ln R&-R^{\lambda_3}&-R^{\lambda_4}\\0&0&0&(1-\nu)&-\lambda_{3\nu}R^{\lambda_3}&-\lambda_{4\nu}R^{\lambda_4}\\1&R_1^2&-1&-\ln R_1&-R_1^{\lambda_3}&-R_1^{\lambda_4}\\0&2R_1^2&0&-1&-\lambda_3R_1^{\lambda_3}&-\lambda_4R_1^{\lambda_4}\\0&2(1+v)R_1^2&0&(1-\nu)&-\lambda_{3\nu}R_1^{\lambda_3}&-\lambda_{4\nu}R_1^{\lambda_4}\\0&0&0&2(1-\nu)&0&0\end{bmatrix},\tag{27}$$

$$\{K_1\}=\begin{Bmatrix}A_{25}R^2+A_{26}R^{m+2}\\2DR^2+2(1+v)A_{25}R^2+m_{\nu1}A_{26}R^{m+2}\\A_{25}R_1^2+(A_{26}-A_{16})R_1^{m+2}\\2A_{25}R_1^2+(m+2)(A_{26}-A_{16})R_1^{m+2}\\2(1+v)A_{25}R_1^2+m_{\nu1}(A_{26}-A_{16})R_1^{m+2}\\Y_1\end{Bmatrix}\tag{28}$$

where $Y_1=2D(1+\overline{R}_1^m)R_1^2+4(1+\nu)A_{25}R_1^2-m(m+2)^2A_{16}R_1^{m+2}+m_{\nu3}A_{26}R_1^{m+2}$ with $m_{\nu3}=(m+2)[m^2+4m+2(1+\nu)]$.

(3) For $n\neq0$ or $n\neq2$

The matrices $[K]$ and $\{K_1\}$ for $n \neq 0$ or $n \neq 2$ are found as:

$$[K] = \begin{bmatrix} 0 & 0 & -1 & -R^{\lambda_2} & -R^{\lambda_3} & -R^{\lambda_4} \\ 0 & 0 & 0 & -\lambda_{2\nu}R^{\lambda_2} & -\lambda_{3\nu}R^{\lambda_3} & -\lambda_{4\nu}R^{\lambda_4} \\ 1 & R_1^2 & -1 & -R_1^{\lambda_2} & -R_1^{\lambda_3} & -R_1^{\lambda_4} \\ 0 & 2R_1^2 & 0 & -\lambda_2 R_1^{\lambda_2} & -\lambda_3 R_1^{\lambda_3} & -\lambda_4 R_1^{\lambda_4} \\ 0 & 2(1+\nu)R_1^2 & 0 & -\lambda_{2\nu}R_1^{\lambda_2} & -\lambda_{3\nu}R_1^{\lambda_3} & -\lambda_{4\nu}R_1^{\lambda_4} \\ 0 & 0 & 0 & -\lambda_{2n}R_1^{\lambda_2} & -\lambda_{3n}R_1^{\lambda_3} & -\lambda_{4n}R_1^{\lambda_4} \end{bmatrix}, \tag{29}$$

$$\{K_1\} = \begin{Bmatrix} A_{25}R^2 + A_{26}R^{m+2} \\ 2DR^2 + 2(1+v)A_{25}R^2 + m_{\nu 1}A_{26}R^{m+2} \\ A_{25}R_1^2 + (A_{26} - A_{16})R_1^{m+2} \\ 2A_{25}R_1^2 + (m+2)(A_{26} - A_{16})R_1^{m+2} \\ 2(1+v)A_{25}R_1^2 + m_{\nu 1}(A_{26} - A_{16})R_1^{m+2} \\ Y_2 \end{Bmatrix} \tag{30}$$

where $\lambda_{2n} = \lambda_2[\lambda_2^2 + (n-2)\lambda_2 - n(1-\nu)]$, $\lambda_{3n} = \lambda_3[\lambda_3^2 + (n-2)\lambda_3 - n(1-\nu)]$, $\lambda_{4n} = \lambda_4[\lambda_4^2 + (n-2)\lambda_4 - n(1-\nu)]$, $m_{\nu 4} = (m+2)[m(m+2) + n(m+1+\nu)$, and $Y_2 = nD(1 + \overline{R}_1^m)R_1^2 + 2n(1+\nu)A_{25}R_1^2 - m(m+2)^2 A_{16}R_1^{m+2} + m_{\nu 4}A_{26}R_1^{m+2}$.

3.4. Numerical Solution

For illustration, let us consider the values $R = 1$ m, $R_1 = (2/3)R$, $h = 0.05$ m, $z = 0.02$ m, $\nu = 0.3$, $E_0 = 210$ GPa, $T_0 = 50$ °C, $\alpha = 1 \times 10^{-5}$/°C. The analytical results were evaluated and subsequently validated using the finite element method. In the finite element analysis, due to the axisymmetric condition, a rectangular surface with dimensions of thickness $h = 0.05m$ and radius $R = 1m$ is selected. The surface is then divided into elements by creating 200 layers along the thickness direction and 60 layers in the radial direction, resulting in a total of 12,000 elements. Eight-node elements are utilized in the finite element mesh. The thermal load and Young's modulus in the mesh are determined based on prescribed functions and vary from layer to layer.

Firstly, let us focus on the variation of the thermal index P. Figure 2 and Table 1 showcase the theoretical and finite element results of the bending stresses for the parameters $n = 2$, $m = 2$ and P takes values of 0, 1, and 2. The results indicate a decreasing trend in stresses as the thermal index P increases. This can be attributed to the fact that with an increase in the P index, the thermal load decreases, thereby leading to a reduction in stresses.

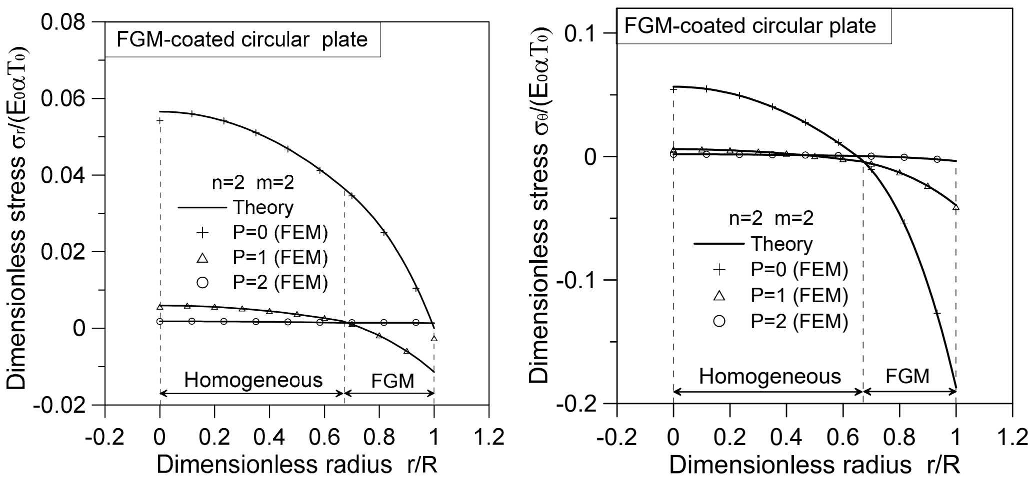

Figure 2. The distributions of stresses σ_r and σ_θ of the radially FGM-coated circular plate ($n = 2$) subjected to radially ($m = 2$) and different transversely thermal loads ($P = 0, 1, 2$).

Table 1. Theoretical and finite element results of the bending stresses $\sigma_r/E_0\alpha T_0$ for $P = 1, 2, 3$.

r/R	Stress $\sigma_r/E_0\alpha T_0$ (P = 0)			Stress $\sigma_r/E_0\alpha T_0$ (P = 1)			Stress $\sigma_r/E_0\alpha T_0$ (P = 2)		
	FEM	**Analytical**	**Error (%)**	**FEM**	**Analytical**	**Error (%)**	**FEM**	**Analytical**	**Error (%)**
0	0.0542001	0.056543	4.144	0.005665	0.005942	4.649	0.001792	0.001816	1.346
0.1	0.0561685	0.056099	0.125	0.005931	0.00585	1.366	0.001845	0.001807	2.093
0.2	0.0547974	0.054765	0.058	0.005651	0.005574	1.383	0.001819	0.00178	2.121
0.3	0.0525399	0.052543	0.006	0.005188	0.005113	1.464	0.001775	0.001736	2.211
0.4	0.0493821	0.049432	0.100	0.004541	0.004469	1.613	0.001714	0.001673	2.347
0.5	0.0453222	0.045432	0.242	0.003709	0.00364	1.884	0.001635	0.001593	2.538
0.6	0.0403602	0.040543	0.451	0.002691	0.002627	2.433	0.001538	0.001496	2.788
0.7	0.0345711	0.034722	0.434	0.001124	0.001036	8.500	0.001478	0.001425	3.610
0.8	0.0266747	0.026978	1.124	−0.00184	−0.00195	5.657	0.001507	0.001434	4.864
0.9	0.0152738	0.015857	3.679	−0.00587	−0.00600	2.081	0.001515	0.001418	6.377
1	0.000000	0.000000	0.000	−0.01256	−0.01143	9.891	0.001446	0.001355	6.289

Moving forward, let us investigate the influence of the material index n on mechanical behavior. Figure 3 presents the stresses for $P = 0$, $m = 2$ and $n = 0, 0.5, 1, 2, 3$. It is evident that as the value of n increases, indicating a decrease in the overall Young's modulus, the stresses decrease accordingly. These results showcased in Figure 3 highlight the effectiveness of utilizing the FGM-coated layer in reducing the maximum stress in the circular plate. Furthermore, Figure 4 depicts the mechanical behavior with fixed values of P and n while varying the parameter m. The plots in Figure 4 demonstrate that the stresses in the homogeneous portion of the FGM-coated circular plate follow a function of r^m, by Equation (18). Additionally, the stresses along the radial direction exhibit continuity with noticeable inflection points at the interfaces, particularly for smaller values of m.

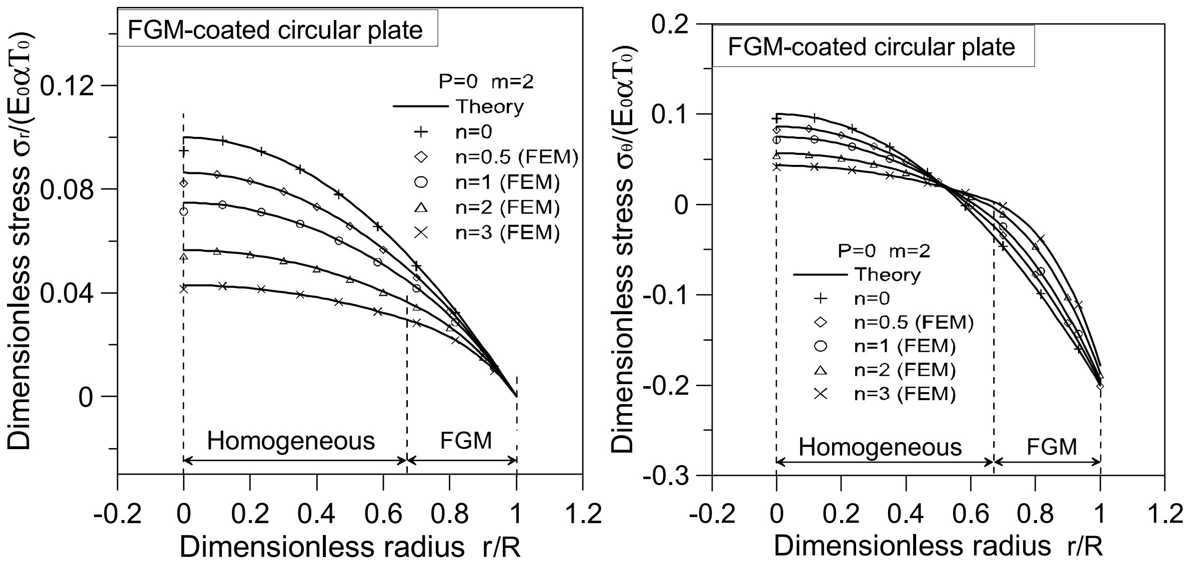

Figure 3. The distributions of stresses σ_r and σ_θ of the radially FGM-coated circular plate with different material index $n = 0$ [34], 0.5, 1, 2, 3 subjected to transversely and radially thermal loads for $P = 0$, $m = 2$.

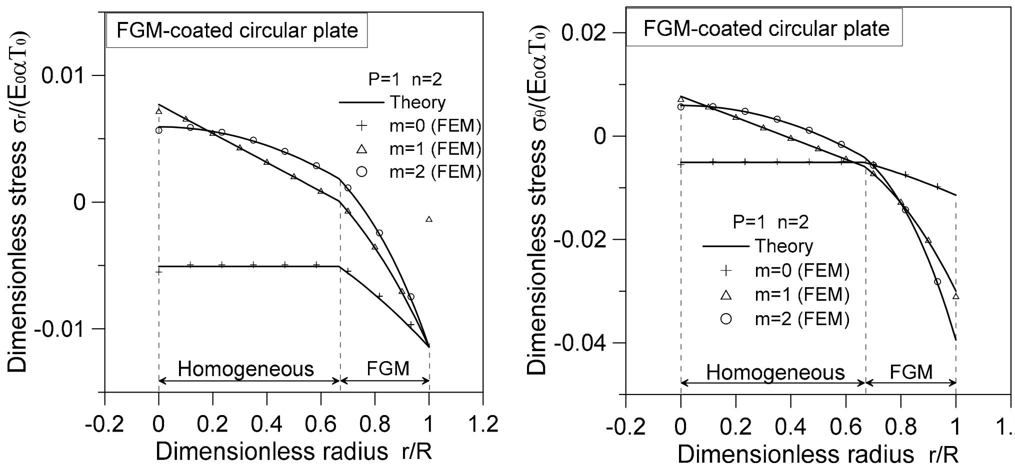

Figure 4. The distributions of stresses σ_r and σ_θ of the radially FGM-coated circular plate ($n = 2$) subjected to different radially thermal loads ($m = 0$, 1, 2).

Furthermore, let us examine how the thickness of the coating influences mechanical behavior. In this analysis, we consider the ratios $R_1/R = 0.1$, 0.2, 0.5, 1. The variations of stresses and moments along the radial direction for these ratios are presented in Figures 5 and 6. The results indicate the following observations: First, smaller values of the ratio R_1/R, corresponding to thicker FGM layers, result in lower stresses. Second, in the case of a homogeneous circular plate ($R_1/R = 1$), the maximum stress or moment is located at the center of the circular plate. However, when the circular plate is coated with a thicker FGM layer (smaller R_1/R), the maximum stress or moment shifts towards the inner part of the FGM-coated circular plate. Third, the stress and bending moment curves exhibit similar patterns, indicating a proportional relationship for certain values of n, m, and P. As mentioned in Section 3.2, the thermal stresses and moments exhibit the relations $M_j = h^3\sigma_j/(12z)$, $j = r, \theta$ for the special case when $P = 0$. These findings shed light on the impact of the coating thickness on the mechanical behavior of the circular plate and provide valuable insights for practical applications.

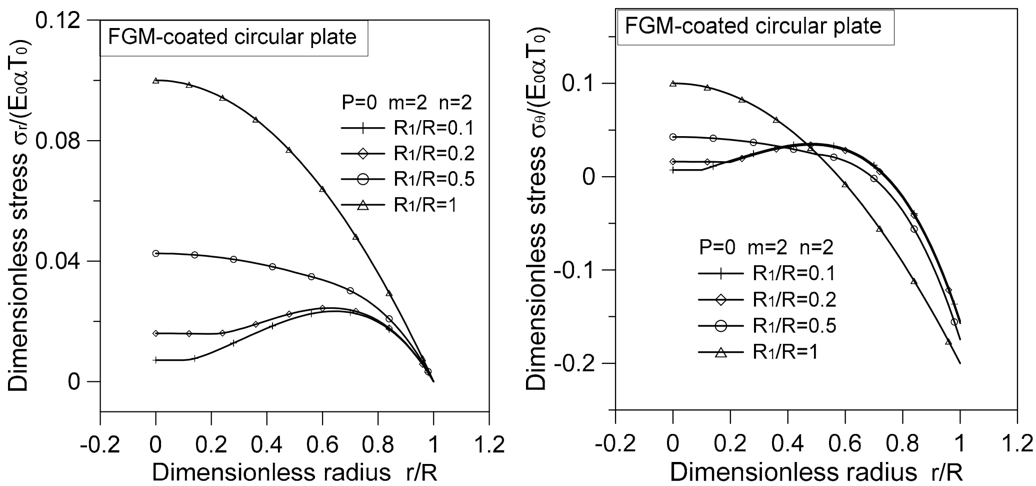

Figure 5. The distributions of stresses σ_r and σ_θ of the radially FGM-coated circular plate ($n = 2$) subjected to thermal load ($P = 0$, $m = 2$) while the coated thickness changes with $R_1/R = 0.1$, 0.2, 0.5, 1.

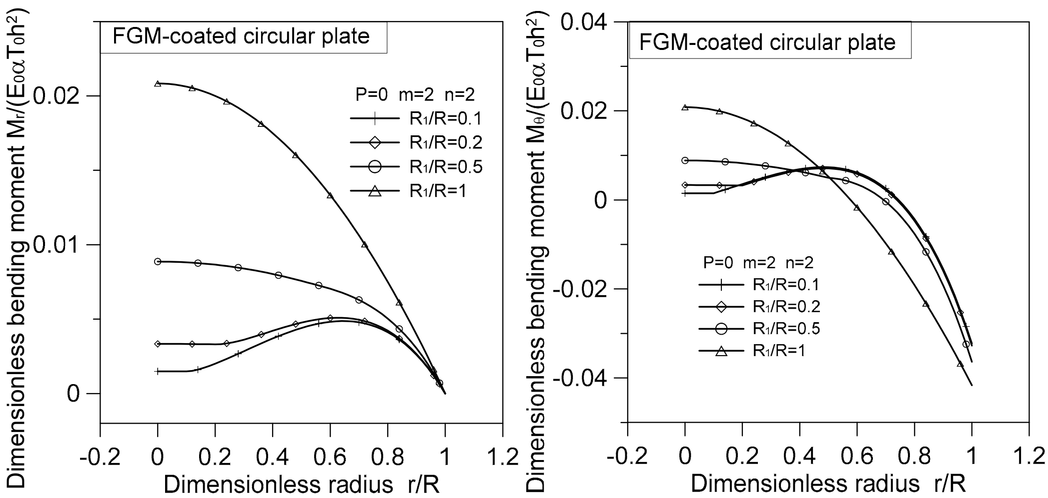

Figure 6. The distributions of bending moments M_r and M_θ of the radially FGM-coated circular plate ($n = 2$) subjected to thermal load ($P = 0$, $m = 2$) when the coated thickness changes with $R_1/R = 0.1, 0.2, 0.5, 1$.

To further analyze the effect of radially applied thermal load on the mechanical behavior of the radially FGM-coated circular plate, let us consider the thermal parameters $P = -0.5$ and $m = 0.5, 1, 2, 3$. It is worth noting that $P = -0.5$ signifies the absence of transverse thermal loads. Figures 7 and 8 present the stresses and bending moments of the FGM-coated circular plate under radially applied thermal load. Observations from Figures 7 and 8 are as follows: Firstly, the stresses of the homogeneous portion of the circular plate are functions of r^m, contributed by the radially applied thermal load. On the other hand, the stresses of the FGM layer follow a polynomial r^{m+n}, influenced by both the radially applied thermal load and material gradation. Consequently, the stresses σ_r and σ_θ in Figure 7 of the radially FGM-coated circular plate subjected only to the radially thermal load ($P = -0.5$) exhibit continuity with noticeable inflection points in slope at the interfaces ($R_1 = 2R/3$). Secondly, for $P = -0.5$, the thermal stresses and moments do not exhibit a proportional relationship.

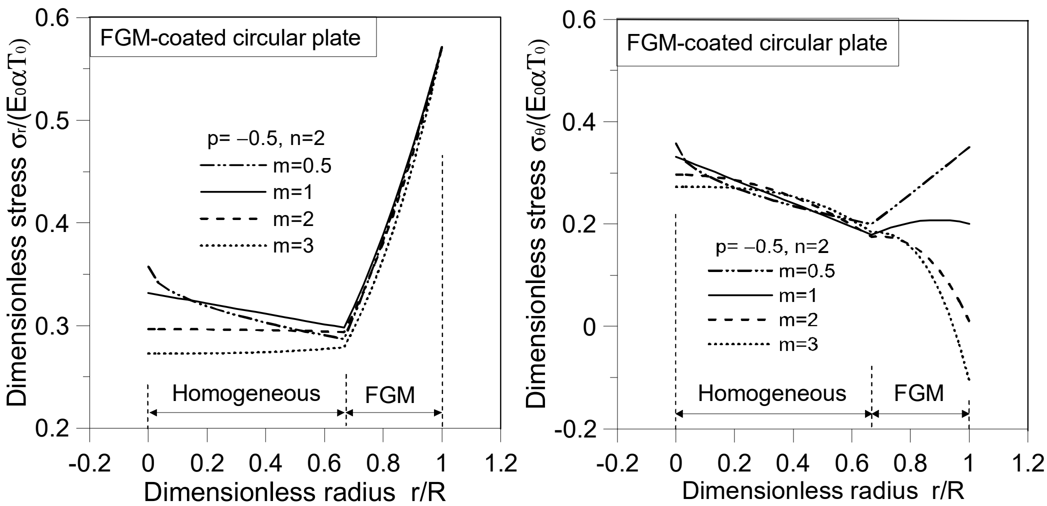

Figure 7. The distributions of the stresses σ_r and σ_θ of the radially FGM-coated circular plate ($n = 2$) subjected to the radially thermal load only ($P = -0.5, m = 0.5, 1, 2, 3$).

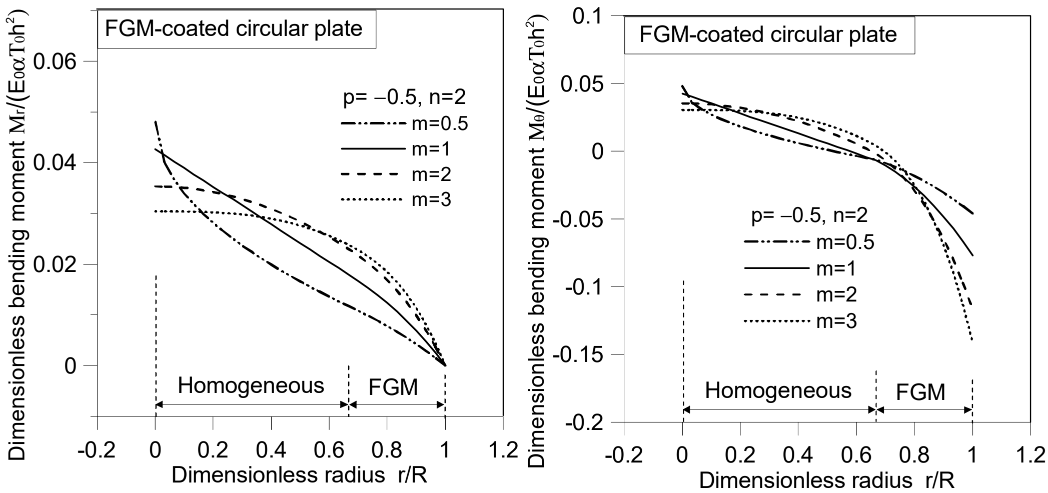

Figure 8. The distributions of bending moments M_r and M_θ of the radially FGM-coated circular plate ($n = 2$) subjected to the radially thermal load only ($P = -0.5$, $m = 0.5,\ 1,\ 2,\ 3$).

Notably, the proposed analytical solution can be applied to a homogeneous circular plate by setting the material index $n = 0$ in the FGM-coated circular plate. When the FGM-coated circular plate degenerates into a homogeneous circular plate ($n = 0$), the stress and moment behaviors under transverse thermal loads ($P = 0,\ 2$) and radial thermal loads ($m = 1,\ 2,\ 3$) are depicted in Figure 9. These results exhibit a dependence on the function r^m for the homogeneous circular plate. Moreover, it is noteworthy that the effects of radial thermal loads are more pronounced compared to transverse thermal loads when the value of P is small. This suggests that radial thermal loads have a greater influence on the mechanical behavior of the radially FGM circular plate.

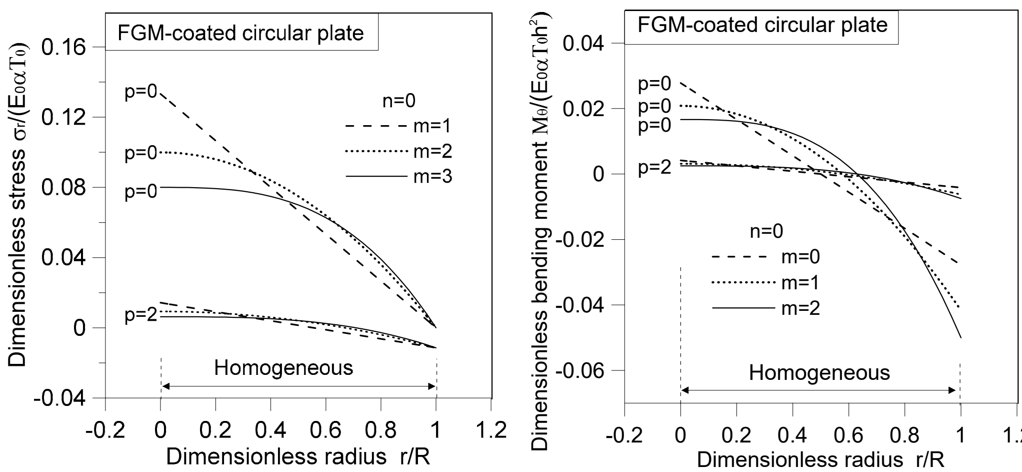

Figure 9. The distributions of stress σ_r and bending moment M_θ of the homogeneous circular plate ($n = 0$) subjected to the transversely and radially thermal load ($P = 0,\ 2$, and $m = 0,\ 1,\ 2$).

4. Circular Plate Undercoated with Radially FGM

The concerned FGM-undercoated circular plate illustrated in Figure 1b is constructed by attaching a homogeneous ring to the outer radius of the FGM-coated circular plate in Section 3. The Poisson's ratio ν is assumed uniform, while Young's modulus of the FGM-undercoated circular plate is

$$E(r) = \begin{cases} E_0(R_1/R_2)^n & 0 \le r < R_1 \\ E_0(r/R_2)^n & R_1 \le r \le R_2. \\ E_0 & R_2 < r \le R \end{cases} \tag{31}$$

Further, assume that the FGM-undercoated circular plate is also subjected to the thermal load $T(r,z) = T_0(1+\bar{r}^m)\bar{z}^{2P+1}$. The general solutions in Section 2 can be applied to the three portions of the FGM-undercoated circular plate, including the homogeneous circular portion in $0 \le r < R_1$, the FGM-undercoated annular portion in $R_1 \le r \le R_2$, and the homogeneous annular portion in $R_2 \le r \le R$.

4.1. The Homogeneous Circular Portion: $0 \le r < R_1$

The findings presented in Section 3.1 are applicable to the homogeneous circular region within the range of $0 \le r < R_1$, with the exception that Young's modulus $E_0^* = E_0(R_1/R)^n$ is substituted with $E_0^* = E_0(R_1/R_2)^n$.

4.2. The FGM-Undercoated Annular Portion: $R_1 \le r \le R_2$

The solution to the FGM-undercoated annular portion in $R_1 \le r \le R_2$ can be found by employing the results in Section 3.2, replacing $E_0^* = E_0(r/R)^n$ by $E_0^* = E_0(r/R_2)^n$.

4.3. The Homogeneous Annular Portion: $R_2 \le r \le R$

The solution fields of the homogeneous annular portion of the FGM-undercoated circular plate in the range $R_2 \le r \le R$ can be evaluated by replacing A_{2j} $(j = 1,6)$ in Equations (19) and (20) by A_{3j} $(j = 1,6)$ and illustrated as follows:

$$w(r) = A_{31} + A_{32}r^2 + A_{33}\ln r + A_{34}r^2\ln r + A_{36}r^{m+2} \text{ for } R_2 < r \le R \tag{32}$$

where $A_{36} = -D/[(m+2)^2R^m]$ for $m \ne 0$; $A_{36} = 0$ for $m = 0$. The stresses and bending moments found by the use of Equation (21) are

$$\begin{aligned} \sigma_r &= -\tfrac{zE_0}{1-\nu^2}\{2(1+\nu)A_{32} - (1-v)A_{33}r^{-2} + [2(1+v)\ln r + 3 + v]A_{34} + m_{\nu 1}A_{36}r^m\} - \sigma_{T1}, \\ \sigma_\theta &= -\tfrac{zE_0}{1-\nu^2}\{2(1+\nu)A_{32} + (1-v)A_{33}r^{-2} + [2(1+v)\ln r + 3v + 1]A_{34} + m_{\nu 2}A_{36}r^m\} - \sigma_{T1}, \\ M_j &= \tfrac{h^3}{12z}\sigma_{j1} - M_{T1}, j = r, \theta. \end{aligned} \tag{33}$$

4.4. The Analytical Solution of the FGM-Undercoated Circular Plate

To obtain the analytical solution for the FGM-undercoated circular plate, it is necessary to ensure that the boundary and continuity conditions at the interfaces between the FGM and the homogeneous layers are met. The boundary conditions are

$$w(r = R) = 0,\ M_r(r = R) = 0 \tag{34}$$

and the continuity conditions are

$$\begin{aligned} & w(r = R_1^-) = w(r = R_1^+),\ w(r = R_2^-) = w(r = R_2^+), \\ & \tfrac{dw}{dr}\Big|_{r=R_1^-} = \tfrac{dw}{dr}\Big|_{r=R_1^+},\ \tfrac{dw}{dr}\Big|_{r=R_2^-} = \tfrac{dw}{dr}\Big|_{r=R_2^+}, \\ & M_r(r = R_1^-) = M_r(r = R_1^+),\ M_r(r = R_2^-) = M_r(r = R_2^+), \\ & V_r(r = R_1^-) = V_r(r = R_1^+),\ V_r(r = R_2^-) = V_r(r = R_2^+). \end{aligned} \tag{35}$$

Setting up the simultaneous equations of the boundary and continuity conditions gives the unknown constants A_{ij} in the form of

$$\{A_{11},\ A_{12},\ A_{21},\ A_{22},\ A_{23},\ A_{24},\ A_{31},\ A_{32},\ A_{33},\ A_{34}\}^T = [K]^{-1}\{K_1\}. \tag{36}$$

The superscript T in Equation (36) denotes the transform and the quantity $[K]^{-1}$ represents the inverse of the matrix $[K]$. The unknown constants A_{ij} will be determined according to the different values of the quantity n as follows:

(1) For $n = 0$

By applying the boundary and continuity conditions for $n = 0$ in Equation (34), we can easily solve for the unknown coefficients A_{ij}. As a result, the bending deflection for the entire circular plate can be determined as follows:

$$w(r) = \frac{DR^2}{2(1+\nu)}\left\{\frac{m+3-v}{m+2}\left(1-\bar{r}^2\right) + \frac{2(1+v)}{(m+2)^2}\left(1-\bar{r}^{m+2}\right)\right\}. \tag{37}$$

when $n = 0$, the FGM-undercoated circular plate becomes a homogeneous circular plate. Therefore, Equation (37) is equivalent to Equation (25) and aligns with the findings of Hetnarski [34], as anticipated.

(2) For $n = 2$

The matrices $[K]$ and $\{K_1\}$ in Equation (36) for $n = 2$ are established as:

$$[K] = \begin{bmatrix} 0 & 0 & 0 & 0 & 0 & 0 & 1 & R^2 & \ln R & R^2\ln R \\ 0 & 0 & 0 & 0 & 0 & 0 & 0 & 2(1+\nu)R^2 & -(1-\nu) & X_1R^2 \\ 1 & R_1^2 & -1 & -\ln R_1 & -R_1^{\lambda_3} & -R_1^{\lambda_4} & 0 & 0 & 0 & 0 \\ 0 & 0 & -1 & -\ln R_2 & -R_2^{\lambda_3} & -R_2^{\lambda_4} & 1 & R_2^2 & \ln R_2 & R_2^2\ln R_2 \\ 0 & 2R_1^2 & 0 & -1 & -\lambda_3R_1^{\lambda_3} & -\lambda_4R_1^{\lambda_4} & 0 & 0 & 0 & 0 \\ 0 & 0 & 0 & -1 & -\lambda_3R_2^{\lambda_3} & -\lambda_4R_2^{\lambda_4} & 0 & 2R_2^2 & 1 & X_3R_2^2 \\ 0 & 2(1+\nu)R_1^2 & 0 & (1-\nu) & -\lambda_{3\nu}R_1^{\lambda_3} & -\lambda_{4\nu}R_1^{\lambda_4} & 0 & 0 & 0 & 0 \\ 0 & 0 & 0 & (1-\nu) & -\lambda_{3\nu}R_2^{\lambda_3} & -\lambda_{4\nu}R_2^{\lambda_4} & 0 & 2(1+\nu)R_2^2 & -(1-\nu) & X_2R_2^2 \\ 0 & 0 & 0 & 2(1-\nu) & 0 & 0 & 0 & 0 & 0 & 0 \\ 0 & 0 & 0 & 2(1-\nu) & 0 & 0 & 0 & 0 & 0 & 4R_2^2 \end{bmatrix} \tag{38}$$

where $X_1 = 3+\nu+2(1+\nu)\ln R$, $X_2 = 3+\nu+2(1+\nu)\ln R_2$, $X_3 = 1+2\ln R_2$, and

$$\{K_1\} = \begin{Bmatrix} -A_{36}R^{m+2} \\ -2DR^2 - m_{\nu1}A_{36}R^{m+2} \\ A_{25}R_1^2 + (A_{26}-A_{26})R_1^{m+2} \\ A_{25}R_2^2 - (A_{36}-A_{26})R_2^{m+2} \\ 2A_{25}R_1^2 + (m+2)(A_{26}-A_{16})R_1^{m+2} \\ 2A_{25}R_2^2 - (m+2)(A_{36}-A_{26})R_2^{m+2} \\ 2(1+v)A_{25}R_1^2 + m_{\nu1}(A_{26}-A_{16}){R_1}^{m+2} \\ 2(1+v)A_{25}R_2^2 - m_{\nu1}(A_{36}-A_{26}){R_2}^{m+2} \\ Y_1 \\ Y_3 \end{Bmatrix} \tag{39}$$

where $Y_3 = 2D(1+\overline{R}_2^m)R_2^2 + 4(1+\nu)A_{25}R_2^2 - m(m+2)^2A_{36}R_2^{m+2} + m_{\nu3}A_{26}R_2^{m+2}$. Subsequently, the unknown constants A_{ij} for $n = 2$ can be evaluated from Equations (36), (38) and (39).

(3) For $n \neq 0$ or $n \neq 2$

With the aid of Equation (36), the matrices $[K]$ and $\{K_1\}$ in Equation (36) for $n \neq 0$ or $n \neq 2$ are

$$[K] = \begin{bmatrix} 0 & 0 & 0 & 0 & 0 & 0 & 1 & R^2 & \ln R & R^2 \ln R \\ 0 & 0 & 0 & 0 & 0 & 0 & 0 & 2(1+v)R^2 & -(1-v) & X_1 R^2 \\ 1 & R_1^2 & -1 & -R_1^{\lambda_2} & -R_1^{\lambda_3} & -R_1^{\lambda_4} & 0 & 0 & 0 & 0 \\ 0 & 0 & -1 & -R_2^{\lambda_2} & -R_2^{\lambda_3} & -R_2^{\lambda_2} & 1 & R_2^2 & \ln R_2 & R_2^2 \ln R_2 \\ 0 & 2R_1^2 & 0 & -\lambda_2 R_1^{\lambda_2} & -\lambda_3 R_1^{\lambda_3} & -\lambda_4 R_1^{\lambda_4} & 0 & 0 & 0 & 0 \\ 0 & 0 & 0 & -\lambda_2 R_2^{\lambda_2} & -\lambda_3 R_2^{\lambda_3} & -\lambda_4 R_2^{\lambda_4} & 0 & 2R_2^2 & 1 & X_3 R_2^2 \\ 0 & 2(1+v)R_1^2 & 0 & -\lambda_{2\nu} R_1^{\lambda_2} & -\lambda_{3\nu} R_1^{\lambda_3} & -\lambda_{4\nu} R_1^{\lambda_4} & 0 & 0 & 0 & 0 \\ 0 & 0 & 0 & -\lambda_{2\nu} R_2^{\lambda_2} & -\lambda_{3\nu} R_2^{\lambda_3} & -\lambda_{4\nu} R_2^{\lambda_4} & 0 & 2(1+v)R_2^2 & -(1-v) & X_2 R_2^2 \\ 0 & 0 & 0 & -\lambda_{2n} R_1^{\lambda_2} & -\lambda_{3n} R_1^{\lambda_3} & -\lambda_{4n} R_1^{\lambda_4} & 0 & 0 & 0 & 0 \\ 0 & 0 & 0 & -\lambda_{2n} R_2^{\lambda_2} & -\lambda_{3n} R_2^{\lambda_3} & -\lambda_{4n} R_2^{\lambda_4} & 0 & 0 & 0 & 4R_2^2 \end{bmatrix} \quad (40)$$

$$\{K_1\} = \begin{Bmatrix} -A_{36} R^{m+2} \\ -2DR^2 - m_{\nu 1} A_{36} R^{m+2} \\ A_{25} R_1^2 - (A_{16} - A_{26}) R_1^{m+2} \\ A_{25} R_2^2 - (A_{36} - A_{26}) R_2^{m+2} \\ 2A_{25} R_1^2 + (m+2)(A_{26} - A_{16}) R_1^{m+2} \\ 2A_{25} R_2^2 - (m+2)(A_{36} - A_{26}) R_2^{m+2} \\ 2(1+v) A_{25} R_1^2 + m_{\nu 1}(A_{26} - A_{16}) R_1^{m+2} \\ 2(1+v) A_{25} R_2^2 - m_{\nu 1}(A_{36} - A_{26}) R_2^{m+2} \\ Y_2 \\ Y \end{Bmatrix} \quad (41)$$

where $Y_4 = nD(1 + \overline{R}_2^m) R_2^2 + 2n(1+\nu) K_{25} R_2^2 - m(m+2)^2 K_{36} R_2^{m+2} + m_{\nu 4} K_{26} R_2^{m+2}$. Therefore, the unknown constants A_{ij} for $n \neq 0$ or $n \neq 2$ can be determined from Equations (36), (40) and (41). Consequently, the deflection, stresses, and moments of the FGM-undercoated circular plate can be evaluated according to the results in Sections 4.1–4.3, after the coefficients A_{ij} are obtained.

4.5. Numerical Solution

By employing the values $R = 1$ m, $R_1 = 0.2R$, $R_2 = 0.8R$, $h = 0.05$ m, $z = 0.02$ m, $\nu = 0.3$, $E_0 = 210$ GPa, $T_0 = 50$ °C, $\alpha = 1 \times 10^{-5}$/°C, the analytical results were assessed and validated using numerical solutions obtained through the finite element method. The stress variations of the FGM-undercoated circular plates are presented in Figure 10 for different P values ($P = 0,\ 1,\ 2$), in Figure 11 for different n values ($n = 0,\ 0.5,\ 1,\ 2,\ 3$), and in Figure 12 for different m values ($m = 0,\ 1,\ 2$).

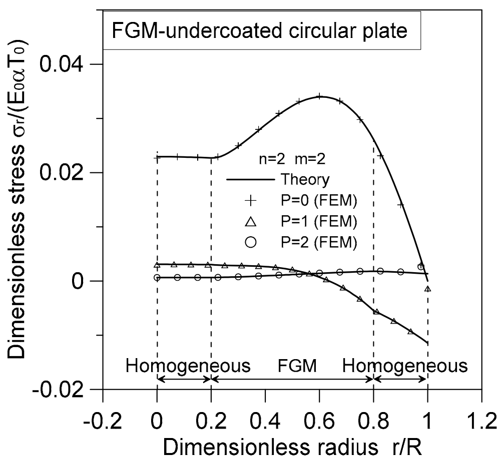

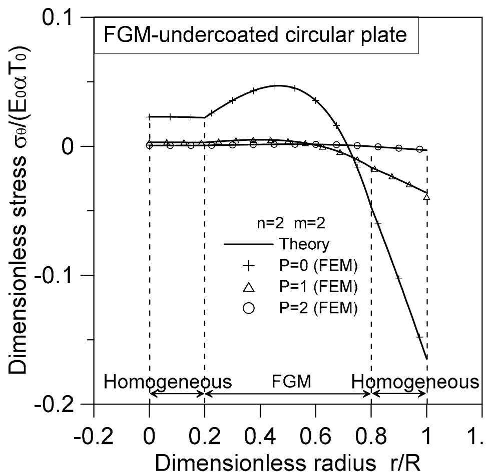

Figure 10. The distributions of stresses σ_r and σ_θ of the radially FGM-undercoated circular plate ($n = 2$) subjected to radially ($m = 2$) and different transversely thermal loads ($P = 0,\ 1,\ 2$).

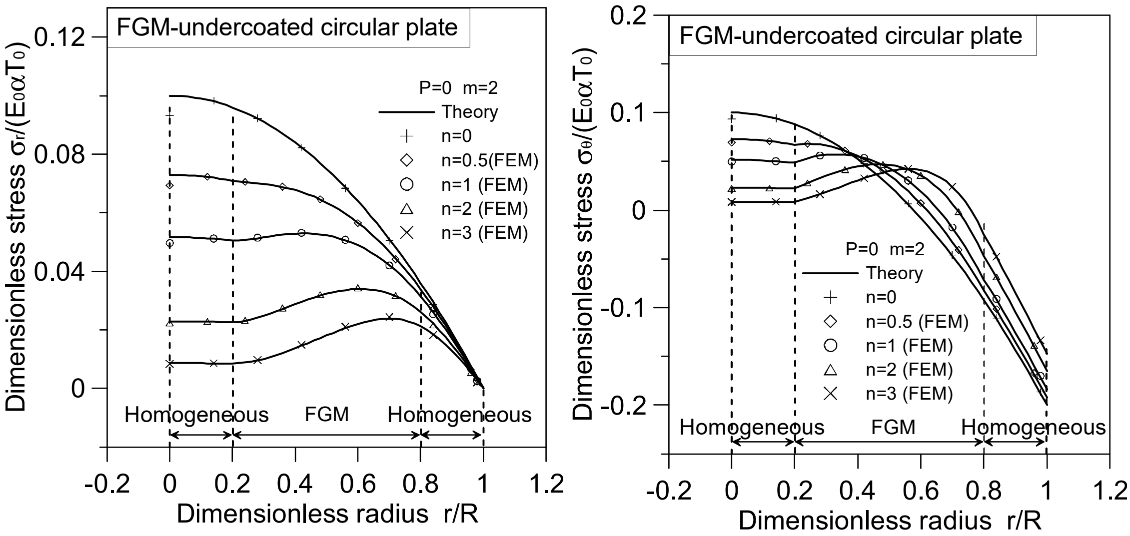

Figure 11. The distributions of stresses σ_r and σ_θ of the radially FGM-undercoated circular plate with different material index $n = 0$ [34], 0.5, 1, 2, 3 subjected to transversely and radially thermal loads for $P = 0, m = 2$.

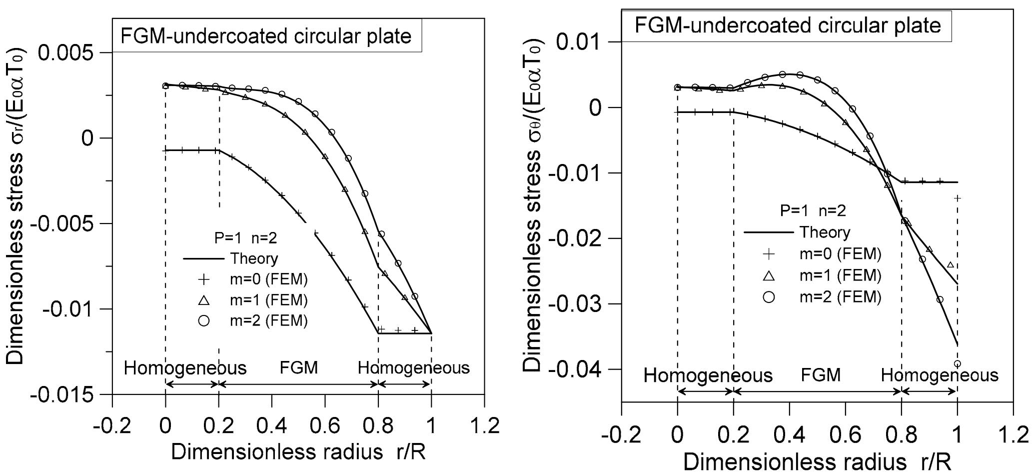

Figure 12. The distributions of stresses σ_r and σ_θ of the radially FGM-undercoated circular plate ($n = 2$) subjected to transversely ($P = 1$) and different radially thermal loads ($m = 0, 1, 2$).

Upon comparing Figures 10–12 to Figures 2–4, respectively, it becomes evident that the mechanical behavior of the FGM-coated circular plate differs from that of the FGM-undercoated circular plate, which is formed by simply adding a homogeneous ring to the outer radius of the former. This difference may be attributed to a squeezing effect caused by the added ring, leading to an increase in stress in the FGM-undercoated layer, particularly for larger values of n and m, as well as smaller values of P. These findings suggest that the addition of a homogeneous layer to an FGM-coated circular plate significantly affects its mechanical response.

Exploring the influence of the FGM-undercoated layer thickness provides an additional intriguing aspect to consider. Figure 13 exhibits the stress distribution of the FGM-undercoated circular plate for different undercoated thicknesses, represented by $R_1/R = 0.1, 0.2, 0.3, 0.5$ and $R_2 = 0.8R$. Notably, a decrease in R_1/R, indicating an increase in FGM-undercoated thickness, corresponds to a decrease in the maximum stress within the FGM-undercoated circular plate. It suggests that thicker FGM-undercoated layers lead to lower maximum stress levels. Furthermore, upon comparing Figures 5 and 13, it is evident that the stress behaviors of both the FGM-coated and FGM-undercoated circular plates exhibit similar patterns.

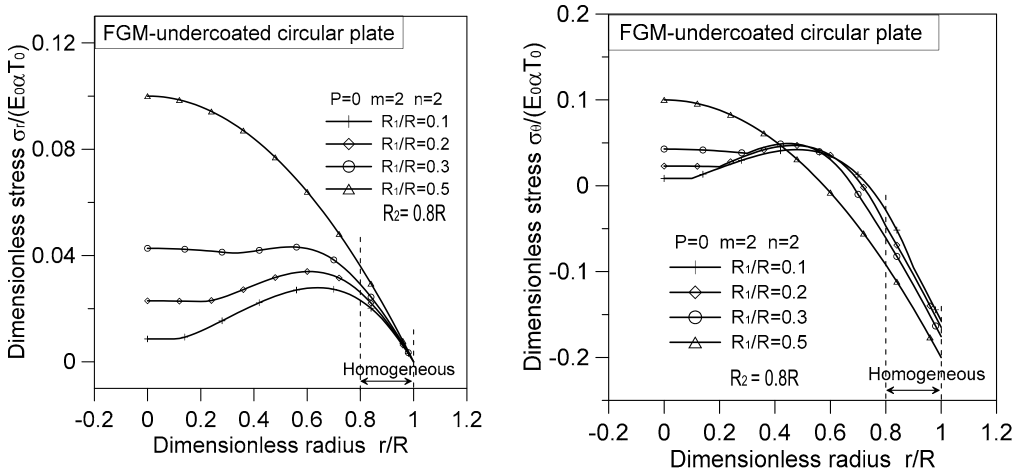

Figure 13. The distributions of stresses σ_r and σ_θ of the FGM-undercoated circular plate ($n = 2$) subjected to thermal load ($P = 0, m = 2$) when the undercoated thickness changes with $R_1/R = 0.1,\ 0.2,\ 0.3,\ 0.5$ and $R_2 = 0.8R$.

5. Conclusions

This study has successfully obtained analytical thermal solutions for radially FGM-coated or FGM-undercoated circular plates subjected to transversely and radially thermal loads, utilizing classical plate theory. The findings lead to the following conclusions:

1. Incorporating FGM as a coated or undercoated layer can effectively reduce the maximum thermal stress experienced by the circular plate. Notably, the maximum thermal stress in the FGM-coated or FGM-undercoated plate is located within the radius of the circular plate ($r \neq 0$), which differs from the behavior observed in homogeneous circular plates.
2. For the case where the index $P = 0$, the thermal stresses and moments of the FGM-coated circular plate under the thermal load $T(r,z) = T_0(1 + \bar{r}^m)\bar{z}^{2P+1}$ demonstrate the proportional relations of $M_j = h^3\sigma_j/(12z),\ j = r,\ \theta$.
3. Under transversely thermal loads ($m = 0$), the stresses at the homogeneous portion of the FGM-coated circular plate remain unaffected by the radius r. However, the stresses at the FGM-ring portion vary depending on the radius, owing to the radially varying material properties of the FGM layer.
4. When subjected to radially thermal loads only ($P = -0.5$), the stresses and moments of the homogeneous portion depend on the product of r^m influenced by the radially thermal load. Conversely, the stresses and moments of the FGM layer are determined by the function r^{m+n}, which takes into account both the thermal load and material gradation.
5. The stresses σ_r and σ_θ of the radially FGM-coated circular plate, whether subjected to transversely thermal load only ($m = 0$) or radially thermal load only ($P = -0.5$), exhibit continuity with noticeable inflection points in slope at the interfaces.
6. The numerical findings obtained from this study can serve as a benchmark for researchers in validating their numerical methods and results when analyzing similar problems involving FGM-coated and FGM-undercoated circular plates.
7. The developed analytical solutions can be applied to analyze the mechanical behavior of various FGM-coated and FGM-undercoated circular plates subjected to different thermal loading conditions. Further investigations can explore their application in specific engineering problems.

Author Contributions: Conceptualization, Y.-L.C.; Methodology, Y.-L.C.; Validation, Y.-L.C.; Formal analysis, Z.-H.L.; Writing—original draft, Y.-L.C.; Project administration, Y.-L.C. All authors have read and agreed to the published version of the manuscript.

Funding: This research received no external funding.

Institutional Review Board Statement: Not applicable.

Informed Consent Statement: Not applicable.

Data Availability Statement: Not applicable.

Conflicts of Interest: The authors declare no conflict of interest.

References

1. Chung, Y.L.; Chi, S.H. The Residual Stresses of Functionally Graded Materials. *J. Chin. Inst. Civ. Hydraul. Eng.* **2001**, *13*, 1–9.
2. Chung, Y.L.; Chang, H.X. Mechanical behavior of rectangular plates with functionally graded coefficient of thermal expansion subjected to thermal loading. *J. Therm. Stress.* **2008**, *31*, 368–388. [CrossRef]
3. Chung, Y.L. Thermoelastic closed-form solutions of FGM plates subjected to temperature change in longitudinal and thickness directions. *Meccanica* **2022**, *57*, 355–369. [CrossRef]
4. Golmakani, M.E.; Kadkhodayan, M. Large deflection analysis of circular and annular FGM plates under thermo-mechanical loadings with temperature-dependent properties. *Compos. Part B Eng.* **2011**, *42*, 614–625. [CrossRef]
5. Dai, H.L.; Yan, X.; Yang, L. Thermoelastic Transient Behavior for a Clamped FGM Circular Plate. *Int. J. Struct. Stab. Dyn.* **2014**, *14*, 1450005. [CrossRef]
6. Parandvar, H.; Farid, M. Nonlinear reduced order modeling of functionally graded plates subjected to random load in thermal environment. *Compos. Struct.* **2015**, *126*, 174–183. [CrossRef]
7. Alibeigloo, A. Thermo elasticity solution of sandwich circular plate with functionally graded core using generalized differential quadrature method. *Compos. Struct.* **2016**, *136*, 229–240. [CrossRef]
8. Ding, S.; Wu, C.P. Optimization of material composition to minimize the thermal stresses induced in FGM plates with temperature-dependent material properties. *Int. J. Mech. Mater. Des.* **2018**, *14*, 527–549. [CrossRef]
9. Zhang, J.H.; Pan, S.C.; Chen, L.K. Dynamic thermal buckling and postbuckling of clamped-clamped imperfect functionally graded annular plates. *Nonlinear Dyn.* **2019**, *95*, 565–577. [CrossRef]
10. Zarga, D.; Tounsi, A.; Bousahla, A.A.; Bourada, F.; Mahmoud, S.R. Thermomechanical bending study for functionally graded sandwich plates using a simple quasi-3D shear deformation theory. *Steel Compos. Struct.* **2019**, *32*, 389–410. [CrossRef]
11. Vaghefi, R. Thermo-elastoplastic analysis of functionally graded sandwich plates using a three-dimensional meshless model. *Compos. Struct.* **2020**, *242*, 112144. [CrossRef]
12. Moleiro, F.; Madeira, J.F.A.; Carrera, E.; Reddy, J.N. Design optimization of functionally graded plates under thermo-mechanical loadings to minimize stress, deformation and mass. *Compos. Struct.* **2020**, *245*, 112360. [CrossRef]
13. Bagheri, H.; Kiani, Y.; Eslami, M.R. Asymmetric thermal buckling of temperature dependent annular FGM plates on a partial elastic foundation. *Comput. Math. Appl.* **2018**, *75*, 1566–1581. [CrossRef]
14. Ghiasian, S.E.; Kiani, Y.; Sadighi, M.; Eslami, M.R. Thermal buckling of shear deformable temperature dependent circular/annular FGM plates. *Int. J. Mech. Sci.* **2014**, *81*, 137–148. [CrossRef]
15. Kiani, Y. Axisymmetric static and dynamics snap-through phenomena in a thermally postbuckled temperature-dependent FGM circular plate. *Int. J. Non-Linear Mech.* **2017**, *89*, 1–13. [CrossRef]
16. Akgöz, B.; Civalek, Ö. Effects of thermal and shear deformation on vibration response of functionally graded thick composite microbeams. *Compos. Part B Eng.* **2017**, *129*, 77–87. [CrossRef]
17. Javani, M.; Kiani, Y.; Eslami, M.R. Large amplitude thermally induced vibrations of temperature dependent annular FGM plates. *Compos. Part B Eng.* **2019**, *163*, 371–383. [CrossRef]
18. Chung, Y.L.; Chen, W.T. Bending behavior of FGM-coated and FGM-undercoated plates with two simply supported opposite edges and two free edges. *Compos. Struct.* **2007**, *81*, 157–167. [CrossRef]
19. Chi, S.H.; Chung, Y.L. Cracking in coating-substrate composites with multi-layered and FGM coatings. *Eng. Fract. Mech.* **2003**, *70*, 1227–1243. [CrossRef]
20. Han, Q.F.; Wang, Z.W.; Nash, D.H.; Liu, P.Q. Thermal buckling analysis of cylindrical shell with functionally graded material coating. *Compos. Struct.* **2017**, *181*, 171–182. [CrossRef]
21. Mao, J.J.; Ke, L.L.; Yang, J.; Kitipornchai, S.; Wang, Y.S. The coupled thermoelastic instability of FGM coatings with arbitrarily varying properties: In-plane sliding. *Acta Mech.* **2018**, *229*, 2979–2995. [CrossRef]
22. Daikh, A.A.; Megueni, A. Thermal buckling analysis of functionally graded sandwich plates. *J. Therm. Stress.* **2018**, *41*, 139–159. [CrossRef]
23. Dung, D.V.; Nga, N.T. Thermomechanical postbuckling analysis of eccentrically stiffened FGM sandwich plates with general Sigmoid and power laws based on TSDT. *J. Sandw. Struct. Mater.* **2018**, *20*, 907–945. [CrossRef]

24. Daikh, A.A.; Drai, A.; Bensaid, I.; Houari, M.S.A.; Tounsi, A. On vibration of functionally graded sandwich nanoplates in the thermal environment. *J. Sandw. Struct. Mater.* **2021**, *23*, 2217–2244. [CrossRef]
25. Nguyen, V.C.; Tran, H.Q.; Pham, V.V. Nonlinear static analysis of bi-directional functionally graded sandwich plates in thermal environments by a higher-order finite element model. *Thin-Walled Struct.* **2023**, *188*, 110819. [CrossRef]
26. Sah, S.K.; Ghosh, A. Influence of porosity distribution on free vibration and buckling analysis of multi-directional functionally graded sandwich plates. *Compos. Struct.* **2022**, *279*, 114795. [CrossRef]
27. Najafizadeh, M.M.; Heydari, H.R. An exact solution for buckling of functionally graded circular plates based on higher order shear deformation plate theory under uniform radial compression. *Int. J. Mech. Sci.* **2008**, *50*, 603–612. [CrossRef]
28. Wan, Z.Q.; Li, S.R.; Li, Q.Q. Homogenized and classical expressions for bending solutions of functionally graded levinson circular plates. *Gongcheng Lixue/Eng. Mech.* **2015**, *32*, 10–16. [CrossRef]
29. Dai, H.L.; Dai, T.; Cheng, S.K. Transient Response Analysis for a Circular Sandwich Plate with an FGM Central Disk. *J. Mech.* **2015**, *31*, 417–426. [CrossRef]
30. Chung, Y.L.; Ou, Z.X. Exact bending solutions of circular sandwich plates with functionally graded material-undercoated layer subjected to axisymmetric distributed loads. *J. Sandw. Struct. Mater.* **2020**, *23*, 2856–2881. [CrossRef]
31. Nie, G.; Zhong, Z. Axisymmetric bending of two-directional functionally graded circular and annular plates. *Acta Mech. Solida Sin.* **2007**, *20*, 289–295. [CrossRef]
32. Sburlati, R. Stress concentration factor due to a functionally graded ring around a hole in an isotropic plate. *Int. J. Solids Struct.* **2013**, *50*, 3649–3658. [CrossRef]
33. Goyat, V.; Verma, S.; Garg, R.K. On the reduction of stress concentration factor in an infinite panel using different radial functionally graded materials. *Int. J. Mater. Prod. Technol.* **2018**, *57*, 109–131. [CrossRef]
34. Hetnarski, R.B. *Thermal Stress I*; Achenbach, J.D., Ed.; North-Holland: New York, NY, USA, 1986.